

Cross-Validation of Open-Path and Closed-Path Eddy-Covariance Techniques for Observing Methane Fluxes

Hiroki Iwata · Yoshiko Kosugi · Keisuke Ono · Masayoshi Mano · Ayaka Sakabe · Akira Miyata · Kenshi Takahashi

Received: 9 August 2013 / Accepted: 19 November 2013 / Published online: 24 December 2013
© Springer Science+Business Media Dordrecht 2013

Abstract Methane (CH_4) fluxes observed with the eddy-covariance technique using an open-path CH_4 analyzer and a closed-path CH_4 analyzer in a rice paddy field were evaluated with an emphasis on the flux correction methodology. A comparison of the fluxes obtained by the analyzers revealed that both the open-path and closed-path techniques were reliable, provided that appropriate corrections were applied. For the open-path approach, the influence of fluctuations in air density and the line shape variation in laser absorption spectroscopy (hereafter, spectroscopic effect) was significant, and the relative importance of these corrections would increase when observing small CH_4 fluxes. A new procedure proposed by Li-Cor Inc. enabled us to accurately adjust for these effects. The high-frequency loss of the open-path CH_4 analyzer was relatively large (11 % of the uncorrected covariance) at an observation height of 2.5 m above the canopy owing to its longer physical path length, and this correction should be carefully applied before correcting for the influence of fluctuations in air density and the spectroscopic effect. Uncorrected CH_4 fluxes observed with the closed-path analyzer were substantially underestimated (37 %) due to high-frequency loss because an undersized pump was used in the observation. Both the bandpass and transfer function approaches successfully corrected this flux loss. Careful determination of the bandpass frequency range or the transfer function and the cospectral model is required for the accurate calculation of CH_4 fluxes with the closed-path technique.

H. Iwata (✉) · Y. Kosugi · A. Sakabe
Graduate School of Agriculture, Kyoto University, Kyoto 606-8502, Japan
e-mail: hiwata@kais.kyoto-u.ac.jp

K. Ono · A. Miyata
National Institute for Agro-Environmental Sciences, Tsukuba, Ibaraki 305-8604, Japan

M. Mano
Graduate School of Horticulture, Chiba University, Matsudo, Chiba 271-8510, Japan

K. Takahashi
Research Institute for Sustainable Humanosphere, Kyoto University, Uji, Kyoto 611-0011, Japan

Keywords Bandpass · Cospectral similarity · High-frequency loss · Rice paddy · Transfer function · Wavelet transform

1 Introduction

Methane (CH_4) is an important greenhouse gas, with a global warming potential per unit mass that is 25 times greater than that of carbon dioxide (CO_2) on a 100-year time scale (Forster et al. 2007). A few pioneering works to determine CH_4 exchange with the eddy-covariance technique (Kaimal and Finnigan 1994; Lee et al. 2004) were reported by Verma et al. (1992), Hovde et al. (1995), and Suyker et al. (1996). Recent advances in laser absorption spectroscopy (Baer et al. 2002; Li-Cor Inc. 2010; Shemshad et al. 2012) have facilitated employments of laser-based CH_4 analyzers in the eddy-covariance approach, and a number of studies have been conducted since then (e.g., Rinne et al. 2007; Sachs et al. 2008; Hendriks et al. 2008; Zona et al. 2009; Tuzson et al. 2010; Dengel et al. 2011; Querino et al. 2011). Fluxes observed using the eddy-covariance technique represent the spatially-“averaged” exchange at the ecosystem scale, and the technique can be applied on a continuous basis. These properties are particularly effective for quantifying the ecosystem-scale CH_4 exchange, since CH_4 has a heterogeneous source/sink distribution (Sachs et al. 2010) that is laborious to cover with chamber observations. Thus, the present technique using the new CH_4 analyzers has the potential to greatly advance our understanding of the CH_4 budget at the ecosystem scale and larger scales.

When applying the eddy-covariance technique for observing CH_4 exchange, there are currently two options regarding the type of gas analyzer: an open-path or a closed-path gas analyzer. Both analyzers have advantages and disadvantages. The open-path analyzer can be installed adjacent to an ultrasonic anemo-thermometer, which enables the high-frequency loss due to signal decorrelation to be minimized. However, the gas density observed with the open-path analyzer is affected by fluctuations in air density (Webb et al. 1980) and by variations in the absorption line shape in the laser absorption spectroscopic measurement caused by changes in temperature, pressure, and water vapour (Gharavi and Buckley 2005; Li-Cor Inc. 2010). Such effects must be appropriately adjusted for. One advantage of the closed-path gas analyzer is that it does not need these adjustments provided that fluctuations of temperature, water vapour concentration, and pressure are negligibly suppressed in the measurement cell. The closed-path gas analyzer requires a relatively large correction of the high-frequency loss caused mainly by the attenuation of turbulent fluctuations in the sampling tubes and an insufficient flushing speed in the measurement cell.

An important point to consider is that the accuracy of the flux must be assured regardless of the type of analyzer employed in the observation. Both the open-path and closed-path CH_4 analyzers still have issues that need to be carefully examined for accurate flux calculations. Because the available open-path CH_4 analyzer, specifically LI-7700 from Li-Cor Inc., has a larger physical path length compared to open-path $\text{CO}_2/\text{H}_2\text{O}$ gas analyzers, the expected larger high-frequency loss must be appropriately corrected. A new adjustment procedure proposed by Li-Cor Inc. (2010) to correct for variations in the absorption line shape needs to be carefully evaluated before it is used in scientific research.

For closed-path CH_4 analyzers, the validity of the widely-used correction approaches for the high-frequency loss should be examined. Closed-path CH_4 analyzers achieve sensitive measurements by detecting the laser absorption by CH_4 in the decompressed measurement cell (Baer et al. 2002; Asakawa et al. 2010; Shemshad et al. 2012). Furthermore, the measurement cell of closed-path CH_4 analyzers has a larger volume compared to closed-path

CO₂ analyzers, and consequently a high flow speed is necessary to flush the cell in a sufficiently short time. These factors necessitate the use of a high power-consuming pump in eddy-covariance observations with closed-path CH₄ analyzers. However, a high power-consuming pump is not always applicable because of power restrictions at a field site or financial limitations, and measurements may have to be made using an undersized pump. The high-frequency loss can be large (up to 30 %) when an undersized pump is used in conjunction with a closed-path CH₄ analyzer (Detto et al. 2011). Thus, it is of practical importance to examine the applicability of correction approaches for the high-frequency loss to such large attenuation.

There are two widely-used correction approaches for high-frequency loss, i.e., the bandpass approach (Högström et al. 1989; Watanabe et al. 2000; Asanuma et al. 2005) and the transfer function approach (Moore 1986; Massman 2000; Ibrom et al. 2007a). The choice of approach to correct the high-frequency loss is rather subjective, although it seems that the transfer function approach has been more commonly used for correcting both CO₂ and CH₄ fluxes (e.g., Aubinet et al. 2001; Kosugi et al. 2007; Rinne et al. 2007; Smeets et al. 2009; Detto et al. 2011; Peltola et al. 2013), due to the simplicity of the calculation. However, the most appropriate approach should be chosen by considering the site characteristics. The transfer function approach may fail to work correctly for non-ideal conditions (Laubach and McNaughton 1998), specifically when the cospectrum does not follow the ideal shape. This suggests that quite a large amount of data may be influenced because atmospheric turbulence is inherently non-stationary, and an arbitrary threshold in a stationary index is often used for data selection. The bandpass approach also has a weakness in that it is not applicable when the flux of the reference scalar is very small, resulting in a large error in the correction (Watanabe et al. 2000). The drawbacks mentioned above were mainly identified for water vapour and CO₂ exchanges, and it should be investigated if these drawbacks also exist in CH₄ flux observations.

One method used to confirm the accuracy of observations is a comparison of the fluxes obtained from open-path and closed-path analyzers, including the post-processing of data. Detto et al. (2011) conducted such a comparison at three sites with different CH₄ source strengths. They demonstrated that CH₄ fluxes determined from both analyzers agreed reasonably well, however the scatter tended to increase at sites with smaller CH₄ sources. The authors used both fast and slow pumps in the experiment and reported that the fast pump slightly over-performed compared to the slow pump, although this comparison was not conducted in a direct manner. Peltola et al. (2013) compared three closed-path CH₄ analyzers and one open-path CH₄ analyzer installed in a fen for flux observation. Although their focus was not a comparison between the open-path and closed-path analyzers, their results demonstrated that fluxes observed with the open-path and the closed-path analyzers agreed reasonably well. Currently, such comparative studies are limited to the two mentioned above. Important factors that affect the accuracy of fluxes may vary between sites, and more comparative studies under different climates and in different eddy-covariance set-ups will provide valuable information. Moreover, the two studies above applied the transfer function approach to correct for the high-frequency loss of fluxes in the closed-path data, and the applicability of the bandpass approach needs to be examined.

In this study, we compared CH₄ fluxes obtained with both open-path and closed-path CH₄ analyzers for the cross-validation with an emphasis on data post-processing, i.e., the flux correction methodology. We evaluated both the bandpass and transfer function approaches for correcting the high-frequency loss of the closed-path CH₄ observation where an undersized pump was used for the whole observation period. We also attempted to clarify the importance of each correction for the open-path eddy-covariance technique, namely the effects of fluctu-

ations in air density, line-shape variations, and also high-frequency loss. The high-frequency loss of the open-path data is generally small, but not negligible. It was explicitly treated in this study, because this underestimation error propagates to the final corrected fluxes for both the open-path and closed-path techniques, and thus affects any comparison between the techniques. On the basis of the results obtained, suggestions for both the open-path and closed-path techniques are made for a reliable evaluation of CH₄ exchange. For this purpose, we analyzed data obtained in a rice paddy field where a large range of CH₄ fluxes was observed. Throughout the paper, conventional micrometeorological notations are used for the coordinate system and wind velocity vectors. The overbar and prime denote time averaging and deviation from the time average, respectively.

2 Observation

2.1 Study Site

The observations were conducted at the Mase paddy site (36°03'N, 140°02'E, 12 m a.s.l) in Tsukuba, Japan, in 2012. The site is one of the AsiaFlux monitoring sites, and energy and CO₂ fluxes are continuously observed there using the eddy-covariance technique (Miyata et al. 2005; Mano et al. 2007). Paddy fields with similar cultivation practices extend for at least 1 km on flat terrain in the direction of the prevailing wind. Rice was transplanted on May 2 and harvested on September 12 2012. The mean density of rice plant was 14.51 bunch m⁻². The growth of rice was monitored with an interval camera and the canopy height, h , was determined. We started the CH₄ observations using the open-path eddy-covariance technique on March 8 2012, and the closed-path CH₄ analyzer was added to the system on June 10 2012. In this study, two months of data obtained in July and August 2012 were analyzed, because a large range of CH₄ fluxes was observed in these months. In this period, h increased from 0.5 m at the beginning of the observation to 1.1 m around August 10. Subsequently, h gradually declined to 1.0 m by the end of the observation period. Further details of the study site have been described by Saito et al. (2005, 2007) and Ono et al. (2008a,b).

2.2 Instrumentation

To observe the turbulent fluctuations of wind velocity and sonic virtual temperature, an ultrasonic anemo-thermometer (DA-600-3TV, Kaijo Sonic, Japan) with a sensor head with a 0.1-m path length (TR-62AX) was installed at the top of a 3-m observation mast. The observation height was 3.35 m. The sensor head of the ultrasonic anemo-thermometer was set to face the direction of the prevailing wind, and the sensor head was installed precisely level. An open-path CH₄ analyzer (LI-7700, Li-Cor Inc., USA) and an open-path infrared CO₂/H₂O gas analyzer (LI-7500, Li-Cor Inc., USA) were installed at the same height as the ultrasonic anemo-thermometer for CH₄ and water vapour concentration measurements. The mirror heaters embedded in the open-path CH₄ analyzer were switched off to prevent any undesired heat interference (Burba et al. 2008). The sensor separation between the ultrasonic anemo-thermometer and the open-path CH₄ analyzer was 0.29 m and that between the ultrasonic anemo-thermometer and the CO₂/H₂O gas analyzer was 0.25 m.

For the closed-path eddy-covariance observations, a closed-path CH₄ analyzer (RMT-200 Fast Methane Analyzer, Los Gatos Research, Inc., USA) was installed in a small, air-conditioned observation shed, and air samples were drawn from the same height as the sensor path of the ultrasonic anemo-thermometer using a 23-m polypropylene tube with an internal

diameter of 4 mm. The air inlet was 0.12 m from the sensor path of the ultrasonic anemometer. A PTFE filter unit (Millex-FH, 0.45 μm , EMD Millipore, Corp., USA) and metal filter unit (B-4F-60, 60 μm , Swagelok, USA) were inserted into the flow line just after the air inlet and at the inlet of the gas analyzer, respectively, to prevent dust contamination of the measurement cell. Fluctuations in the water vapour concentration of the sampled air were suppressed using a Nafion dryer (PD-50T-24, Perma Pure, Inc., USA) and a reflux method; i.e., the exhaust gas from the CH_4 analyzer was used as the dry purge gas for the dryer. A dry scroll vacuum pump (SH-110, Agilent Technologies, Inc. USA) was placed at the end of flow line. The flow rate was approximately 10 L min^{-1} when connected to the closed-path system; the cell flushing time was estimated as 2.4 s using the cell volume of 0.4 L. All turbulence signals were recorded at 10 Hz by a datalogger (CR1000, Campbell Scientific Inc., USA).

The zero offset of the ultrasonic anemo-thermometer was carefully examined and found to be negligible (less than $\pm 0.02 \text{ m s}^{-1}$). The changes in sensitivity of both the closed-path and open-path CH_4 analyzers were checked with standard gases at the end of this observation. The shift of sensitivity was approximately 1 % for both analyzers. The LI-7500 was replaced with an alternative LI-7500 on April 28 2013, as part of a regular maintenance regime. Before the replacement, the alternative LI-7500 was calibrated with standard gases in a laboratory.

Relevant micrometeorological measurements were also made in the vicinity of the observation mast. The observations included air temperature and relative humidity (HMP-45A, Vaisala, Finland) at a height of 3.35 m, soil and water temperature (copper-constantan thermocouple) at several depths, solar radiation (CMP-6, Kipp & Zonen, The Netherlands) at 2.1 m, and precipitation (TE525MM, Texas Electronics, USA). Half-hourly averages of these variables were recorded by a datalogger (CR3000, Campbell Scientific, Inc., USA).

3 Data Analysis

The raw 10-Hz data were divided into 30-min intervals, and all data analyses and flux calculations were performed on these 30-min data. The following data processing was performed before calculating the covariances. First, data spikes were removed (Vickers and Mahrt 1997); second, a lateral wind correction on the sonic virtual temperature, T_{sv} (K) (Schotanus et al. 1983) was applied. Third, time lags in the signals from different analyzers were corrected by shifting the 10-Hz data. Fourth, a coordinate rotation was performed so that $\bar{v} = 0$ and $\bar{w} = 0$ for all data.

Time lags in the signals from different analyzers occur due to the different speeds of signal processing and the spatial separations between the analyzers. For the closed-path analyzer, the travelling time for sampled air in the tube also needs to be considered. Signals from the open-path $\text{CO}_2/\text{H}_2\text{O}$ gas analyzer and both the open- and closed-path CH_4 analyzers were synchronized to those from the ultrasonic anemo-thermometer for each series of 30-min data using time lags estimated as follows. The time lag was first evaluated for each data series with a cross-correlation analysis (Moncrieff et al. 1997) against T_{sv} from the ultrasonic anemo-thermometer. For the open-path analyzers, relationships between the time lag and wind speed and direction were established. The estimated time lag from the wind speed and direction was then used for signal synchronization for each data series. For the closed-path CH_4 analyzer, the time lag depended on relative humidity (Ibrom et al. 2007b); however its relationship with wind speed and direction was not obvious. Hence, the time lag was determined from relative humidity only. The calculated time lag was typically 9.5 s,

which was approximately in agreement with an estimated time lag from the flow rate and the volume within the sampling tube.

In the following sections, data analyses specific to the open-path and closed-path data are described. We adopted empirical approaches to determine the shape of the transfer functions and the cospectral model whenever possible to eliminate the uncertainty related to the applicability of theoretical models, and to focus on the framework of the flux correction methodology.

3.1 Open-Path Data Processing

3.1.1 Corrections for Air Density Fluctuation and Line shape Variation

The covariance between w and CH_4 molar density observed with the open-path analyzer, m_o (mol m^{-3}), must take into account the effect of fluctuations in air density (Webb et al. 1980) and variations in the CH_4 absorption line shape (Gharavi and Buckley 2005). Hereafter, the latter is referred to as the spectroscopic effect. These corrections were performed in a combined manner (Li-Cor Inc. 2010; McDermitt et al. 2011) as shown below,

$$\overline{w'm'_{oc}} = A \left\{ \overline{w'm'_o} + B \frac{\overline{m_o}}{\rho_d} \overline{w'q'} + C \left(1 + \frac{\overline{q}}{\rho_d} \right) \frac{\overline{m_o}}{\overline{T}} \overline{w'T'} \right\}, \quad (1)$$

where $\overline{w'm'_{oc}}$ is the corrected CH_4 flux, ρ_d is the molar density of dry air (mol m^{-3}), and q is the water vapour molar density (mol m^{-3}). The coefficients, A , B , and C , arise from the correction of the spectroscopic effect and are calculated from air pressure, air temperature (T), and q using the parametric equations of Li-Cor Inc. (2010). The covariance $\overline{w'T'_{sv}}$ was converted to $\overline{w'T'}$ using q (Schotanus et al. 1983) and $\overline{w'T'}$ was used in Eq. 1. The effect of fluctuations in static pressure (Massman and Tuovinen 2006; Li-Cor Inc. 2010) was neglected herein.

3.1.2 Corrections for High-Frequency Loss

Before applying the correction above, high-frequency loss in the open-path system due to sensor separation and line averaging must also be determined to avoid error propagation into the final corrected flux through Eq. 1. In this study, we developed an empirical procedure to correct for the high-frequency loss for the open-path system, to avoid uncertainties related to the applicability of theoretical correction. A widely-used transfer function and time constants in the analytical formulations in Massman (2000) did not recover cospectra with the ideal $-7/3$ power law in the high-frequency region for our data. One reason for this may be that we used the wavelet transform to calculate cospectra, rather than a traditional Fourier transform.

The empirical procedure that we established used look-up tables for the parameters used in one type of transfer function depending on wind speed and lateral sensor separation. The high-frequency loss of $w'T'_{sv}$ was assumed to be negligible, and any attenuation of cospectra of w and signals from the open-path analyzers was evaluated against the cospectra of w and T_{sv} . As will be shown later, the cospectrum of w and T_{sv} has indiscernible high-frequency loss. In this study, the signals from different sensors were synchronized, which thus minimized the effect of longitudinal separation. Other sources of loss, such as the line averaging and phase shifts (Shaw et al. 1998), if any, were accounted for in a bulk manner using this empirical correction.

The transfer function between w and an arbitrary variable, x , denoted as $H_{wx}(f)$ was defined as follows,

$$H_{wx}(f) = \frac{1}{1 + \alpha f^\gamma}, \quad (2)$$

where f is the frequency (s^{-1}). The parameter α is related to the lower end of the frequency band that is affected by the high-frequency loss, e.g., α is greater when the high-frequency loss extends to the lower frequency region. γ expresses the sharpness of the decrease in the transfer function in the high-frequency range; e.g., γ is greater for a sharper decrease in the transfer function. The parameters α and γ were determined for data groups that were defined according to classes of wind speed and lateral separation between the ultrasonic anemo-thermometer and gas analyzers. Different look-up tables for the $\text{CO}_2/\text{H}_2\text{O}$ analyzer- and the CH_4 analyzer-anemometer combination were determined, because the gas analyzers have different sensor path lengths and different sensor separations from the ultrasonic anemo-thermometer.

This correction was applied on both a covariance and cospectrum basis in a consistent manner. To correct covariances, a correction factor, ϵ , was calculated as

$$\epsilon = \frac{\int_0^\infty \widehat{C}^*(f) df}{\int_0^\infty H_{wx}(f) \widehat{C}^*(f) df}, \quad (3)$$

using the transfer function defined in Eq. 2 and a normalized cospectral model \widehat{C}^* (defined below in Eq. 7). Observed covariances were multiplied by ϵ . To correct cospectra, the high-frequency loss was estimated by multiplying the transfer function (Eq. 2) with the cospectral model (Eq. 7), and then the frequency-dependent loss components were added to the observed cospectrum. The use of the same transfer function and cospectral model to correct both covariances and cospectra enabled an accurate comparison of fluxes between the open-path and closed-path technique. This was especially important for the water vapour flux, because the water vapour flux or the cospectrum of w and q appeared in both the air density and spectroscopic effect corrections for the open-path data and the correction of high-frequency loss for the closed-path data with the bandpass approach described in the next section. In this study, the maximal overlap discrete wavelet transform (Percival and Walden 2000) was used to calculate the cospectra (Appendix 1).

3.2 Closed-Path Data Processing

In this measurement, temperature fluctuations were dampened as air travelled through the long sampling tube (Leuning and Judd 1996; Rannik et al. 1997). The fluctuation of the water vapour concentration was also suppressed with a Nafion dryer. It was then assumed that the remaining small fluctuations in temperature, water vapour concentration, and pressure, had a negligible effect on the CH_4 density observed with the closed-path analyzer. Consequently, the closed-path data only needed to be corrected for the high-frequency loss, which is described below.

3.2.1 Bandpass Approach

The bandpass approach utilizes the “local” cospectral similarity between scalars over the higher frequency region, and substitutes high-frequency components of the attenuated signal obtained from a slow-response analyzer with the signal obtained from an analyzer with an ideal frequency response. In this study, the scalar of interest for the high-frequency loss

correction was the CH_4 molar density measured with a closed-path analyzer denoted by m_c (mol m^{-3}),

$$\overline{w'm'_{cc}} = \int_0^{f_2} C_{wm_c}(f)df + \beta \int_{f_2}^{\infty} C_{wr}(f)df, \quad (4)$$

where $\overline{w'm'_{cc}}$ is the corrected CH_4 flux, and C_{wx} is the cospectrum of w and an arbitrary scalar variable, x . f_2 is the frequency above which high-frequency loss affects the cospectrum, and f_2 defines the high-frequency end of the bandpass region. The attenuated $C_{wm_c}(f)$ for $f > f_2$ is replaced with $C_{wr}(f)$, where r indicates a reference scalar with no high-frequency loss. β is the cospectral ratio for the bandpass frequency region and is defined as below,

$$\beta = \frac{\int_{f_1}^{f_2} C_{wm_c}(f)df}{\int_{f_1}^{f_2} C_{wr}(f)df}, \quad (5)$$

where f_1 is the low-frequency end of the bandpass region, and at frequencies below f_1 cospectral similarity does not always hold due to the influence of mesoscale atmospheric motions such as entrainment at the top of the atmospheric boundary layer (Asanuma et al. 2007) and mesoscale circulations related to surface condition contrasts (Saito et al. 2007).

In this study, f_1 and f_2 were determined by examining the ratios between the normalized cospectrum of w and T_{sv} and that of w and m_c . The cospectral ratio was calculated following Kosugi et al. (2007, their Eq. 3 and 4); f_1 and f_2 were determined from the whole dataset, and thus were fixed for the whole analysis period.

The ‘‘local’’ cospectral similarity at higher frequencies is an acceptable assumption over a surface with homogeneous source/sink distributions. However, in practice, there are situations when the similarity does not hold. When the magnitude of the flux of the reference scalar, r , becomes negligibly small, the similarity no longer holds, because the cospectral shape becomes noisy and may not have a noticeable peak for negligible turbulence transfer. This may result in a large correction error. To avoid this situation, r was selected sequentially from T_{sv} , q , and CO_2 (denoted as c) by judging the magnitude of coherence between m_c and r (Eq. 10). First, the coherence between m_c and T_{sv} averaged over the bandpass region was checked and if the averaged coherence was greater than a threshold value, T_{sv} was selected as r . Otherwise, q or c was examined sequentially for the appropriate r in the same way. In this study, C_{wq} and C_{wc} were corrected for the high-frequency loss using the method described in Sect. 3.1, so q and c can be the appropriate r in the bandpass approach. The threshold value was chosen to be 0.5 in this study.

3.2.2 Transfer Function Approach

The fraction of the underestimation due to the high-frequency loss from the ideal cospectral shape can be expressed by the transfer function, $H(f)$. The measured covariance obtained from a slow-response analyzer can then be expressed as follows,

$$\overline{w'm'_{cc}} = \int_0^{\infty} H_{wm_c}(f)C_{wm_c}^*(f)df, \quad (6)$$

where $C_{wm_c}^*(f)$ is the ideal cospectrum without the high-frequency loss.

The normalized version of $C_{wm_c}^*$ was determined empirically by fitting the cospectral model below to $\widehat{C}_{wT_{sv}}$ data, assuming cospectral similarity between m_c and T_{sv} ,

$$\widehat{C}^*(n) = \begin{cases} \frac{an}{(1+bn)^c} & n < n_c \\ \frac{dn}{(1+en)^{7/3}} & n \geq n_c \end{cases} \quad (7)$$

where $a, b, c, d,$ and e are fitting parameters. The subscripts are omitted because it is assumed that the cospectra of w and any scalars are expressed by Eq. 7; n is the normalized frequency, $n \equiv f(z-d)/\bar{u}$, and n_c is determined arbitrarily. The zero-plane displacement, d , was calculated as $0.75h$. Data were separated into groups according to the atmospheric stability, $\zeta \equiv -(z-d)/L_O$, where L_O is the Obukhov length, and the cospectral model was fitted to each group: $\zeta < 0, 0 \leq \zeta < 0.1, 0.1 \leq \zeta < 0.3, 0.3 \leq \zeta < 0.5, 0.5 \leq \zeta < 1.0,$ and $1.0 \leq \zeta$.

The same form of transfer function as Eq. 2 was empirically determined by fitting Eq. 2 to the cospectral ratio between the normalized cospectrum of w and T_{sv} and that of w and m_c as described above. One set of parameters (α and γ) was determined again for the closed-path CH₄ eddy-covariance system, and these parameters were fixed for the whole analysis period.

The correction factor, ϵ , was calculated using Eq. 3. When the observation height is fixed, the ϵ can be determined from $\bar{u}, \zeta,$ and d , once the parameters in Eqs. 2 and 7 are determined appropriately.

3.3 Data Quality Control

All 10-Hz raw data were visually checked and data resulting from instrumental malfunction were discarded. Data with many spikes, abnormal skewness and kurtosis, and large discontinuities were also discarded (Vickers and Mahrt 1997). A stationary test (Mahrt 1998) was used to reject data with strong non-stationarity. Data collected during rainfall were also removed from the analysis.

For specific analyses, such as determining the transfer function (Eq. 2), the bandpass frequency region with the cospectral ratios (i.e., f_1 and f_2), and the cospectral model (Eq. 7), the data were screened with more strict criteria. Data collected during period of large wind speeds and large fluxes were selected using the criteria below: $\bar{u} > 1.0 \text{ m s}^{-1}, |\overline{w'T'_{sv}}| > 0.01 \text{ K m s}^{-1}, |\overline{w'q'}| > 1.0 \text{ mmol m}^2 \text{ s}^{-1},$ and $|\overline{w'm'_c}| > 10 \text{ nmol m}^2 \text{ s}^{-1}$. To determine Eq. 2 for the open-path data, the criterion for \bar{u} was omitted.

4 Results and Discussion

4.1 Corrections of Open-Path Data

4.1.1 High-Frequency Loss

The high-frequency loss of open-path data was corrected on the basis of the covariance and cospectrum as described in Sect. 3.1.2. The parameters in the transfer function (Eq. 2) were determined for the wind speed and lateral separation classes. The parameters α and γ clearly varied with wind-speed classes (Fig. 1): α decreased with increasing wind speed, and γ increased with increasing wind speed. α was generally higher for the CH₄ analyzer-anemometer combination; however the dependence on wind speed was qualitatively the

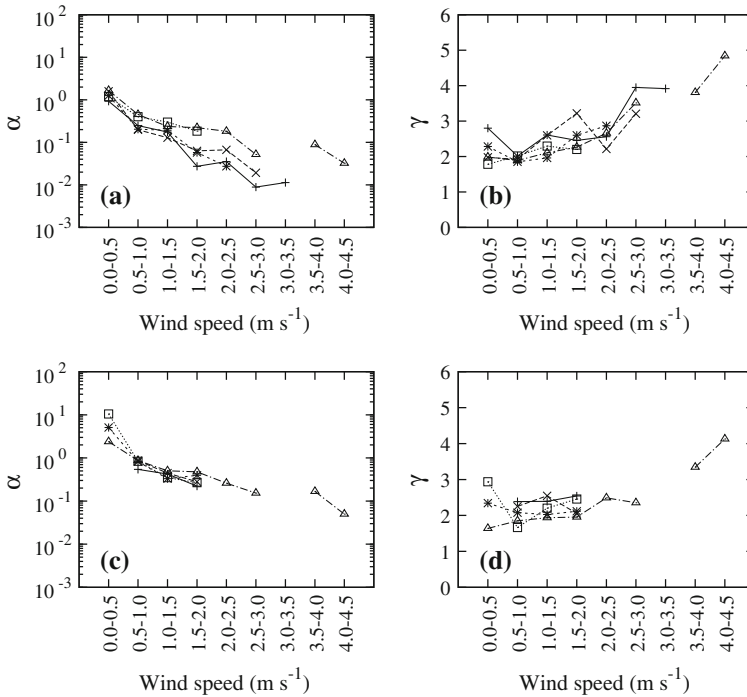


Fig. 1 Variations of the α and γ parameters in the transfer function (Eq. 2) for wind-speed classes for (a and b) the $\text{CO}_2/\text{H}_2\text{O}$ analyzer-anemometer combination and (c and d) the CH_4 analyzer-anemometer combination. Symbols indicate different lateral separation classes: plus for 0.00–0.05 m, times for 0.05–0.10 m, asterisks for 0.10–0.15 m, open square for 0.15–0.20 m, and triangle for 0.20–0.30 m

same for both the $\text{CO}_2/\text{H}_2\text{O}$ analyzer- and CH_4 analyzer-anemometer combinations. This behaviour of α can be explained by the theoretical transfer function of line averaging (Gurvich 1962; Silverman 1968; Kaimal et al. 1968; Horst 1973) and sensor separation (Irwin 1979; Kristensen and Jensen 1979); i.e., the high-frequency loss extends to the lower frequency region with decreasing wind speed, and thus α increases. The larger α for the CH_4 analyzer-anemometer combination can be interpreted as the high-frequency loss affecting the lower frequency region for the larger sensor path length of the CH_4 analyzer. Another parameter γ had approximately the same value for both the $\text{CO}_2/\text{H}_2\text{O}$ analyzer- and the CH_4 analyzer-anemometer combinations for all wind-speed classes. The larger γ in the higher wind-speed classes may reflect the effect of aliasing (Stull 1988). In high wind conditions, the cospectral peak is shifted to a higher frequency, and as a result a larger contribution may exist at frequencies higher than the Nyquist frequency. This affects the shape of the high-frequency region in the cospectrum of w and T_{sv} to a greater degree compared to the cospectrum of w and a scalar with a sensor separation, because this aliasing has a less significant effect on attenuated signals (Laubach and McNaughton 1998). This may result in a sharper decrease in the transfer function at high frequency, thus producing a larger γ with increasing wind speed.

In contrast to the wind-speed dependence, the dependence of the parameters on the lateral separation was less obvious. The parameter α for the $\text{CO}_2/\text{H}_2\text{O}$ analyzer-anemometer combination tended to become larger with increasing lateral separation, whereas the dependence of α on lateral separation for the CH_4 analyzer-anemometer combination and γ for both the

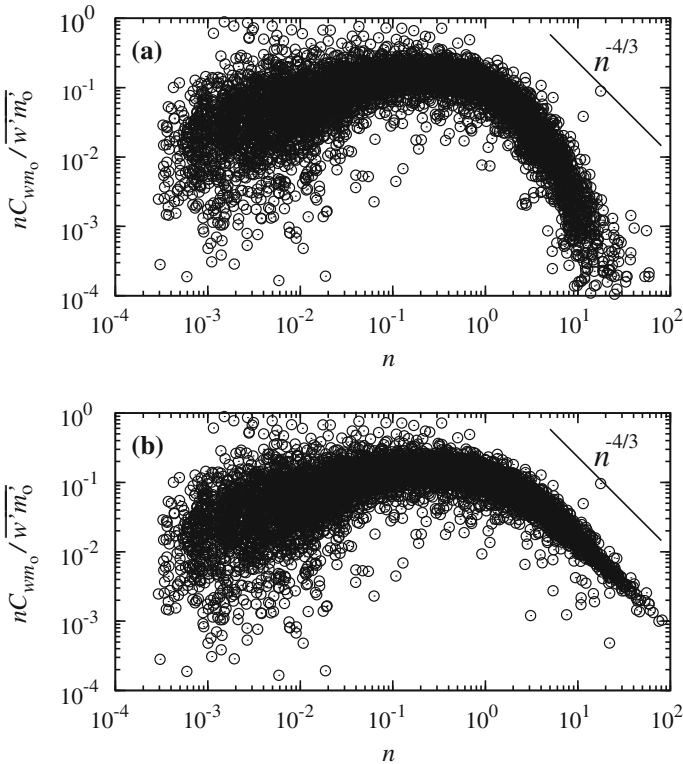


Fig. 2 **a** Observed normalized cospectra of vertical wind speed, w , and CH_4 concentration observed with the open-path gas analyzer, m_0 , and **b** normalized cospectra corrected for the high-frequency loss

combinations were indiscernible. The dependence of α on the lateral separation can also be explained by the theoretical transfer function of sensor separation (Irwin 1979; Kristensen and Jensen 1979). However, the long physical path length of the CH_4 analyzer might have masked the dependence of α on the lateral separation. We designed the instrumentation so that the ultrasonic anemo-thermometer faced into the prevailing wind direction, and the gas analyzers were installed in the lateral direction so that they did not block the anemometer. This resulted in less data for smaller lateral separations, and thus a larger uncertainty for situations with smaller lateral separation.

In practice, α for the $\text{CO}_2/\text{H}_2\text{O}$ analyzer-anemometer combination were grouped into two lateral separation classes separated by 0.15 m. Values were averaged and then a look-up table was created; i.e., α for the $\text{CO}_2/\text{H}_2\text{O}$ analyzer-anemometer combination were determined for two lateral separation and nine wind-speed classes. Other parameters (i.e., α for the CH_4 analyzer-anemometer combination and γ for both combinations) were averaged for each wind-speed class, and one parameter regardless of lateral separation was determined for each wind-speed class. With these empirical transfer functions and the cospectral model obtained in Eq. 7, cospectral loss in the high-frequency region was corrected for the open-path eddy-covariance system. The corrected cospectra were in close agreement to the $-7/3$ power law in the higher frequency range (Fig. 2), indicating an adequate performance for this correction. The magnitude of the correction was 7% for both $\overline{w'q'}$ and $\overline{w'c'}$, and 11% for $\overline{w'm'_0}$ against the uncorrected covariances.

The magnitude of the high-frequency loss correction for $\overline{w'm'_0}$ was also reported by [Peltola et al. \(2013\)](#), who found the high-frequency loss to be 3.5 % against the uncorrected covariance at an observation height of 2 m above the canopy when measured with an ultrasonic anemometer vertically separated upward by 0.45 m. [McDermitt et al. \(2011\)](#) and [Dengel et al. \(2011\)](#) did not report the fractional magnitude of this correction; however their spectra indicate that the magnitude of this correction may be similar to our own at a similar observation height above the canopy. The reason why the high-frequency loss found by [Peltola et al. \(2013\)](#) was smaller than in our study (11 %) is unclear, because a larger separation of the LI-7700 instrument from the ultrasonic anemometer should lead to a larger high-frequency loss. It should be noted that [Peltola et al. \(2013\)](#) used a prototype of the LI-7700 analyzer, and its application was confined to a period of relatively low CH₄ fluxes of about 9 nmol m⁻² s⁻¹ due to instrumental malfunction.

4.1.2 Influence of the Fluctuations of Air Density and the Spectroscopic Effect

The effect of fluctuations in air density and line shape variation on measured $\overline{w'm'_0}$ were adjusted using the covariances corrected for the high-frequency loss as described above to avoid error propagation to the final corrected flux. The effects of these corrections, along with the high-frequency loss correction, on the flux were examined throughout their diurnal variations (Fig. 3).

The observed uncorrected CH₄ flux was smaller during daytime than at nighttime, with the minimum occurring around 0900 (Fig. 3a). The high-frequency loss correction increased the flux with a slightly larger correction applied during nighttime when stable conditions prevailed.

The conventional correction for the air density fluctuation mostly affected the daytime flux (Flux with HFL+WPL in Fig. 3a). This correction contributed to approximately 21 % of the fully corrected fluxes (Flux with HFL+WPL+SS in Fig. 3a) during daytime (Table 1a). The magnitude of the correction for a unit energy transfer was larger for the sensible heat flux, H , as implicitly suggested by [Webb et al. \(1980\)](#). However, in a rice paddy field, the latent heat flux, LE , is the dominant energy transport (Fig. 3b), which resulted in a larger magnitude of the correction term related to LE during daytime. On a typical sunny day, a large latent heat flux cools the surface, resulting in a lower H in the afternoon and even downward H in the late afternoon. This has an important consequence for the correction of the effect of air density fluctuation on $\overline{w'm'_0}$: the correction related to H was greatly reduced in the afternoon, and the total absolute correction was smaller than that in the late morning when the magnitude of correction was at a maximum. Conversely, the correction contributed -4 % during nighttime due to the dominant effect of the downward H (Table 1a).

The effect of the spectroscopic correction was evident only during daytime with an average contribution of 9 % to the fully corrected flux (Table 1a). During nighttime, this correction had an indiscernible effect, and the correction for the air density fluctuation dominated. [Peltola et al. \(2013\)](#) reported corrections for the fluctuation of air density and the spectroscopic effect to be 80 and 24 % as a percentage of the uncorrected covariance, respectively. These values were larger than the values reported by them (recalculated as 40 and 16 % as a percentage of the uncorrected covariance for the fluctuations of air density and the spectroscopic effect, respectively). Their application of the LI-7700 analyzer was confined to a period of relatively low CH₄ fluxes of about 9 nmol m⁻² s⁻¹, and thus their values were larger than the values reported here.

To evaluate the contribution of the high-frequency loss to the final corrected flux, the correction for the fluctuation of air density and the spectroscopic effect was made without

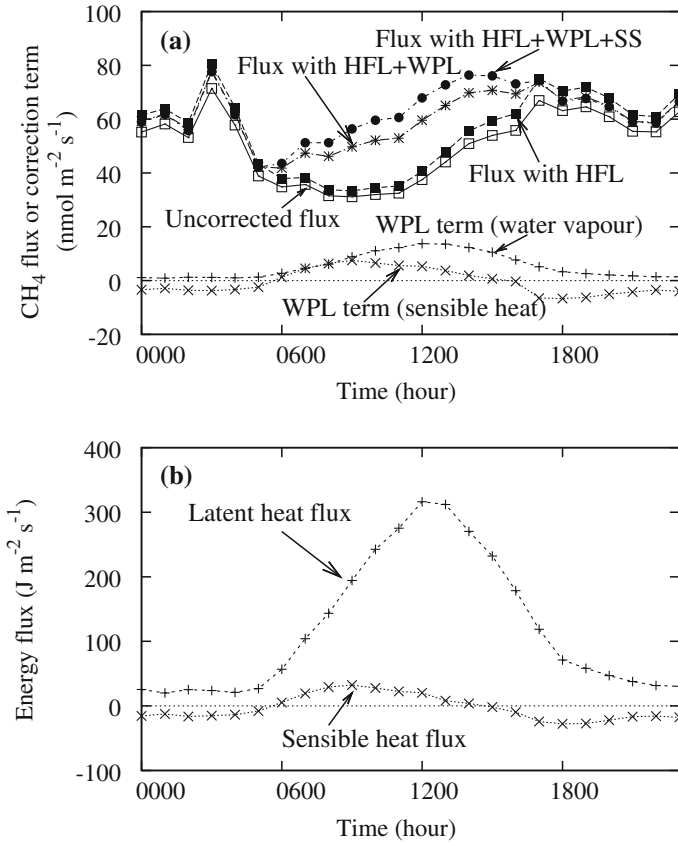


Fig. 3 **a** Mean diurnal variations in uncorrected CH_4 flux observed with the open-path gas analyzer and fluxes with different corrections applied in stages (*HFL* high-frequency loss correction, *WPL* correction for the fluctuations of air density, and *SS* spectroscopic correction), along with the correction terms relating to the fluctuations in air density (denoted as the *WPL* term). **b** Mean diurnal variations of the sensible and latent heat fluxes. Data obtained in July were averaged

applying the high-frequency loss correction to $\overline{w'm'_0}$ and $\overline{w'q'}$ (data not shown). These contributions were typically 6 and 10% of the fully corrected flux for daytime and nighttime respectively (Table 1a). The high-frequency loss of $\overline{w'm'_0}$ dominated this contribution and less than 1% of the fully corrected flux was affected by the high-frequency loss of $\overline{w'q'}$.

The fully corrected CH_4 flux exhibited an emission peak during 1400–1500 and the minimum occurred during 0500–0600 when values were averaged, which is likely to be a consequence of the diurnal variation of soil temperature. Another short-time peak was also observed around 0300, which may correspond to a flush of CH_4 stored within the rice canopy during calm nighttime conditions.

4.2 Corrections to Closed-Path Data and Comparison with Open-Path Data

Herein, an undersized pump was used with the closed-path CH_4 eddy-covariance system. This led to a relatively large underestimation of the CH_4 flux observed with the closed-path system due to the high-frequency loss: the uncorrected CH_4 flux was underestimated by 37% relative to the fully corrected flux obtained from the open-path data (Fig. 4a). This

Table 1 Averaged contribution of various corrections to the final corrected flux for (a) open-path, and (b) closed-path data

	Daytime (0800–1800)	Nighttime (2000–0600)
(a) Open-path data		
HFL of $\overline{w'm'_o}$ (%)	6	10
HFL of $\overline{w'q'}$ (%)	<1	<1
SS (%)	9	<1
WPL (%)	21	–4
$\overline{w'm'_{oc}}$ ($\text{nmol m}^{-2} \text{s}^{-1}$)	66.8	60.6
H (W m^{-2})	10.8	–15.3
LE (W m^{-2})	228.3	28.9
T ($^{\circ}\text{C}$)	27.6	23.0
(b) Closed-path data		
HFL of $\overline{w'm'_c}$ (%)	34	38
$\overline{w'm'_{cc}}$ ($\text{nmol m}^{-2} \text{s}^{-1}$)	65.9	58.5

The contributions were averaged separately for daytime and nighttime. Averaged CH_4 fluxes, sensible heat flux (H), latent heat flux (LE), and air temperature (T) are also shown

HFL high frequency loss, SS spectroscopic correction, WPL air density fluctuation correction

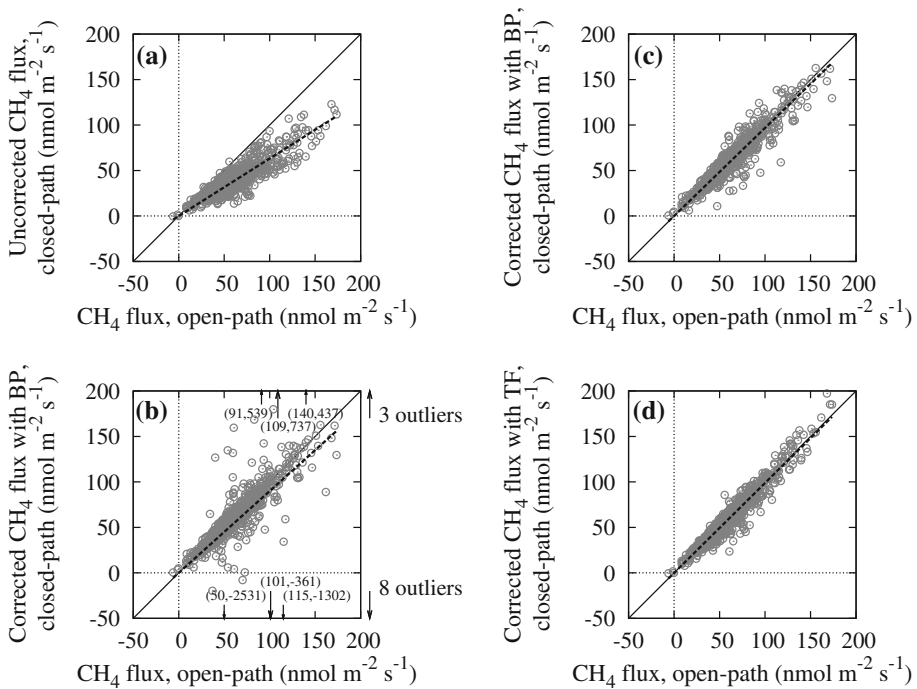


Fig. 4 Comparisons of CH_4 fluxes obtained from the closed-path data (y-axis) against the corrected CH_4 fluxes from the open-path data (x-axis). The flux from the closed-path data were **a** uncorrected, **b** corrected with the bandpass approach (denoted as BP) with only T_{sv} as a reference scalar, **c** corrected with BP with either T_{sv} or q , or c as a reference scalar, and **d** corrected with the transfer function approach (denoted as TF). Data obtained in July are shown. The broken lines are regression lines: **a** $y = 0.63x$ ($R^2 = 0.77$), **b** $y = 0.90x$ ($R^2 = 0.05$), **c** $y = 0.97x$ ($R^2 = 0.88$), and **d** $y = 0.99x$ ($R^2 = 0.93$)

underestimation was slightly larger during nighttime (Table 1b). The bandpass and transfer function approach was applied to correct CH₄ fluxes obtained from the closed-path system. The corrected CH₄ fluxes were compared with the corrected fluxes obtained from the open-path system as described in Sect. 4.1 to evaluate the performance of the bandpass and transfer function approaches, temporarily assuming that the flux based on the open-path data was correct.

4.2.1 Bandpass Approach

In the application of the bandpass approach, the bandpass region needs to be determined in advance. The cospectral ratio was close to unity and the scatter was relatively small between 0.01 and 0.04 Hz (Fig. 5). This indicates that “local” cospectral similarity holds over this frequency region. The high-frequency end of the bandpass region, f_2 , was determined so that the bandpass region was not affected by the attenuation due to the slow response of the closed-path system for CH₄. The cospectral ratio began to decline above 0.04 Hz and was close to zero above 1.0 Hz. As the frequency fell below 0.01 Hz, the scatter became progressively larger, although the median value of the cospectral ratio remained close to unity until 0.002 Hz. Below this frequency, the median value started to deviate from unity. This suggests that cospectral similarity does not always hold below 0.01 Hz at this site. Hence, f_1 and f_2 were determined to be 0.01 and 0.04 Hz, respectively.

The corrected fluxes were compared with fluxes calculated from data obtained with the open-path system. When the bandpass approach was applied with only T_{sv} as the reference scalar, most of the data were corrected to agree with the flux calculated from open-path data (Fig. 4b). However, the scatter was large with some extreme outliers. When other scalars were substituted for T_{sv} in situations where the coherence between T_{sv} and m_c in the bandpass region was lower than the threshold as described in Sect. 3.2.1, the scatter was highly reduced and the corrected CH₄ flux agreed well with the flux observed by the open-path system (Fig. 4c). Of the data, 14 % were calculated based on q , and there were no situations where c was used. In this figure, only the data obtained in July are shown, but the result was also qualitatively the same for August. The root-mean-square error (RMSE) was $9.8 \text{ nmol m}^{-2} \text{ s}^{-1}$

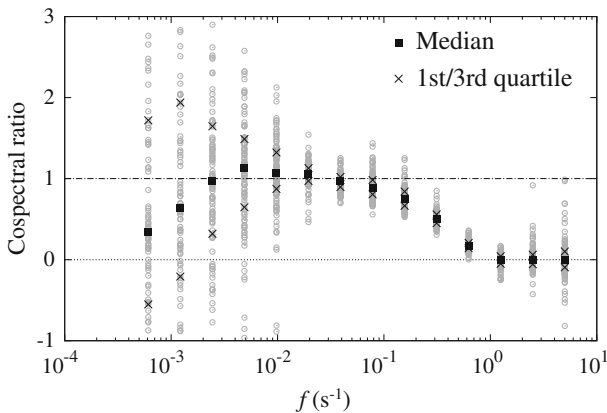


Fig. 5 The ratio of the cospectra of vertical wind velocity, w , and CH₄ concentration observed with the closed-path analyzer, m_c , to the cospectra of w and sonic virtual temperature, T_{sv} , against frequency, f

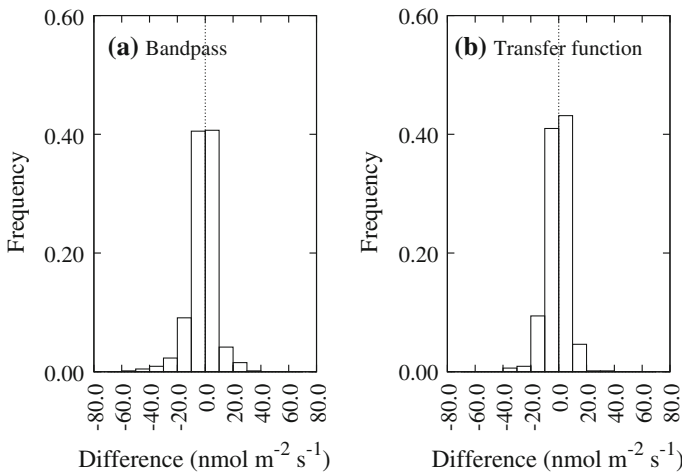


Fig. 6 The distribution of differences between CH_4 fluxes obtained from the open-path and closed-path data in July. CH_4 fluxes from the closed-path data were corrected with **a** the bandpass, and **b** transfer function approaches. The differences were calculated as fluxes from the open-path data minus fluxes from the closed-path data

Table 2 Sensitivity analysis for a widening of the bandpass frequency region

	Base f_1 and f_2	Higher f_2	Lower f_1
Slope	0.97	0.94	0.98
R^2	0.88	0.93	0.85
$RMSE$	9.8	8.3	11.2

f_1 and f_2 indicate the lower and higher ends of the bandpass frequency region, respectively. The unit $RMSE$ is $\text{nmol m}^{-2} \text{s}^{-1}$

for the July data, and the histogram of errors (Fig. 6a) showed that approximately 80% of the data were within $10 \text{ nmol m}^{-2} \text{s}^{-1}$ different.

For the bandpass approach, it is important that the bandpass frequency region, namely f_1 and f_2 , is properly determined. We examined the consequence of widening the bandpass frequency region (Table 2). When f_2 was increased to include one additional higher frequency, the slope decreased to 0.94, although R^2 increased and the $RMSE$ decreased. In this case, a part of the cospectrum close to the higher end of the bandpass region was affected by the high-frequency loss, resulting in the underestimation of β , and thus the fluxes were systematically underestimated. The higher R^2 and lower $RMSE$ probably stemmed from the reduction in random errors in β by averaging a wider bandpass frequency. When f_1 was decreased to include one additional lower frequency, the slope did not vary; however R^2 decreased and $RMSE$ increased. Expanding the bandpass frequency region to a lower frequency resulted in a part of the bandpass region being affected by a failure of cospectral similarity at the lower end in some cases, and as a result the random error in β was increased and $RMSE$ increased.

Saito et al. (2007) reported that cospectral gaps ranging from $\kappa z = 3 \times 10^{-3}$ to 1×10^{-1} , where $\kappa = 2\pi f/\bar{u}$, were observed at the same site, which corresponds to approximately $f = 3 \times 10^{-4}$ to $1 \times 10^{-2} \text{ s}^{-1}$ assuming $\bar{u} = 2 \text{ m s}^{-1}$. The f_1 obtained in this study approximately agrees with the higher frequency end of the distribution of cospectral gaps of

Table 3 The cospectral model obtained for each stability range

Stability range	Lower frequencies	Higher frequencies	n_c
$\zeta < 0$	$6.11n/(1 + 17.82n)^{1.43}$	$0.52n/(1 + 1.18n)^{7/3}$	1.5
$0 \leq \zeta < 0.1$	$3.44n/(1 + 9.23n)^{1.43}$	$1.11n/(1 + 1.52n)^{7/3}$	0.5
$0.1 \leq \zeta < 0.3$	$2.41n/(1 + 5.63n)^{1.43}$	$1.23n/(1 + 1.54n)^{7/3}$	0.5
$0.3 \leq \zeta < 0.5$	$1.05n/(1 + 1.35n)^{1.43}$	$1.21n/(1 + 1.29n)^{7/3}$	0.5
$0.5 \leq \zeta < 1.0$	$0.89n/(1 + 1.33n)^{1.43}$	$1.19n/(1 + 1.28n)^{7/3}$	0.5
$1.0 \leq \zeta$	$1.11n/(1 + 2.37n)^{1.43}$	$1.15n/(1 + 1.23n)^{7/3}$	0.5

n_c divides the data into lower and higher frequencies. n is the normalized frequency

Saito et al. (2007), thus implying that the source of cospectral dissimilarity in the lower frequency in this study is also due to mesoscale transport related to land-surface characteristics at the mesoscale.

4.2.2 Transfer Function Approach

When applying the transfer function approach, the cospectral shape must be precisely modelled. A cospectral model (Eq. 7) was fitted to the observed cospectra between w and T_{sv} (Fig. 7). The fitted cospectral models are listed in Table 3. The cospectral peak occurred around $n = 0.1$ for $\zeta < 0$, and the peak frequency increased as the stable stratification strengthened from $\zeta = 0$ to $\zeta = 0.5$. The cospectra had a broader shape for unstable stratification and became narrower as the stable stratification became greater. These properties are qualitatively identical to those reported by Kaimal et al. (1972). For cospectra in stable stratification, a single curve model has often been used (Moore 1986). However the cospectral models with two separate frequency ranges fitted our data better. Parameter c in Eq. 7 did not vary with the stability, and hence c was fixed to the value of $\zeta < 0$ ($c = 1.43$).

The transfer function, $H(f)$, was empirically determined by fitting Eq. 2 to the median data in Fig. 5. The parameters α and γ were determined to be 11.2 and 1.95, respectively. The effective time constant of the closed-path system was about 2.6 s. This effective time constant was greater than the estimated cell flushing time of 2.4 s, since other factors such as fluctuation damping in the sampling tube affect the total system response.

Corrected fluxes using the transfer function (Eq. 2) and the cospectral model (Eq. 7) were compared with fluxes obtained from the open-path system (Fig. 4d). The corrected fluxes agreed well with fluxes obtained from the open-path system; $RMSE = 6.8 \text{ nmol m}^{-2} \text{ s}^{-1}$. Approximately 80% of the data were within $10 \text{ nmol m}^{-2} \text{ s}^{-1}$ different using the transfer function approach (Fig. 6b). Again, only data obtained in July are shown in this figure, but the result was qualitatively the same for August.

4.3 Suggestions for Eddy-Covariance Applications

The comparison between the open-path and closed-path data suggests that both eddy-covariance techniques for CH_4 are reasonably consistent provided that the necessary corrections are appropriately applied (Fig. 4). The open-path CH_4 data are greatly affected by the fluctuations in air density and the spectroscopic effect. However, the correction proposed by Li-Cor Inc. (2010) allowed us to take these effects into account. The high-frequency loss for the fluxes used in this adjustment should be corrected beforehand. This is particularly

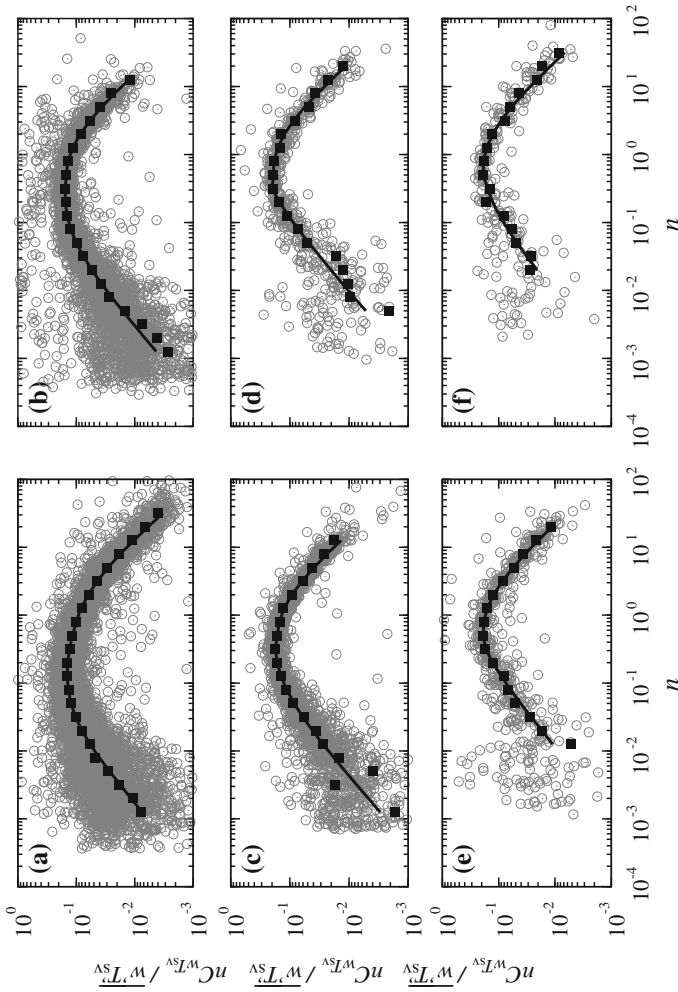


Fig. 7 Cospectra of w and T_{sv} for stability classes: **a** $0.1 \leq \zeta < 0.3$, **b** $0 \leq \zeta < 0.1$, **c** $0.1 \leq \zeta < 0.3$, **d** $0.3 \leq \zeta < 0.5$, **e** $0.5 \leq \zeta < 1.0$, and **f** $1.0 \leq \zeta$. The grey open circles represent all data and the filled squares represent median values in certain normalized frequency bands. The cospectral models (Eq. 7) are fitted to median values and are indicated by curves

critical when applying the open-path CH₄ analyzer to sites with small CH₄ fluxes, such as upland forest ecosystems. When the true CH₄ flux is small, the relative importance of correcting for the fluctuations in air density and the spectroscopic effect increases, and as a result the observed (i.e., uncorrected) CH₄ flux using the open-path analyzer also becomes larger compared to the true flux, in terms of the absolute magnitude. In this case, small errors due to the high-frequency loss of the open-path data may be amplified, in a relative sense, compared to the final corrected flux, through the correction for the fluctuations compared to air density and the spectroscopic effect. This would also be true for the water vapour flux when the true CH₄ flux is small. Hence, the high-frequency loss of observed CH₄ and water vapour fluxes measured with the open-path analyzers, as well as sensible heat flux if any, should be carefully accounted for.

The high-frequency loss of the CH₄ flux observed with the closed-path eddy-covariance technique in this study was relatively large. This is attributable to the use of an under-sized pump. Nevertheless, the corrections applied, i.e., the bandpass and transfer function approaches, satisfactorily accounted for the loss. This may be an important result from a practical perspective because an expensive and high power-consuming pump is not always applicable in field experiments. However, efforts to increase the flow speed may improve the accuracy of the CH₄ flux by reducing the fraction of the flux to be corrected.

In the correction of the closed-path data, the bandpass and transfer function approaches both worked well in our experiment. The histogram of errors (Fig. 6) revealed that both approaches have a similar error distribution. The bandpass approach produced a larger negative difference compared to the transfer function approach. The skewness of the error distribution was -1.01 and -0.38 for the bandpass and transfer function approaches, respectively. Thus, both approaches adequately corrected the high-frequency loss of CH₄ fluxes measured with the closed-path analyzer for quality control data in our dataset, with a slightly better performance when using the transfer function approach.

When applying the bandpass approach, an appropriate reference scalar must be chosen. In most cases, sonic virtual temperature has been used as the reference scalar because of the approximately ideal frequency response of the ultrasonic anemo-thermometer (e.g., Grelle and Lindroth 1996; Yasuda and Watanabe 2001), and for the water vapour flux, there is often no alternative to the sonic virtual temperature. Currently, in most situations where CH₄ flux observations are to be made, turbulence observations for H₂O and CO₂ are available. Therefore, the possibility of these scalars being used as the reference scalar should be considered, as was the case in our study. This is particularly important for the CH₄ flux, because the major sources of CH₄ are wetland areas and rice paddy fields (Schlesinger and Bernhardt 2013), where sonic virtual temperature may not be the appropriate reference scalar owing to the dominance of the latent heat flux in the energy balance.

Another key piece of data processing in both approaches may be the accurate synchronization of CH₄ and wind velocity signals. This enables the convergence of the characteristics of high-frequency loss into a single transfer function. Otherwise, uncertainty will propagate to the final corrected fluxes through the determination of β in the bandpass approach and the transfer function itself in the transfer function approach. The time lag of the CH₄ signal observed with the closed-path analyzer varied with the relative humidity in this study, as reported by Ibrom et al. (2007b). This effect is probably important in humid climates, and must be treated with care. In addition, the bandpass frequency region and the shape of cospectra should be precisely determined.

We initially anticipated that the bandpass approach might be an improvement for correcting the high-frequency loss in the closed-path system based on the results of Laubach and McNaughton (1998). Each cospectrum for 30-min data generally deviates from the com-

posite cospectral shape for atmospheric turbulence. Thus the uncertainty of the modelled cospectra may enhance the uncertainty of the transfer function approach, and the bandpass approach may have an advantage in this respect. Against our expectations, the transfer function approach performed reasonably well, and actually performed slightly better than the bandpass approach. The analysis above was applied to selected data with a stationary index, which might result in a better performance of the transfer function approach. However, we also applied the correction to data with a less strict stationary check, and found that the results were qualitatively unchanged, and the transfer function approach was better. Part of the reason for this may be that our observational site was ideal regarding the homogeneity of wind and scalar source fields; CH₄ emission may be fairly homogeneous in the horizontal direction in an inundated paddy field. Whether the bandpass approach or the transfer function approach is better probably depends on site conditions. The selection of the approach for the high-frequency loss of the closed-path eddy-covariance system should be made carefully for each observational site. This is important considering that flux observations are increasingly conducted worldwide including at sites with less ideal micrometeorological conditions for flux observations.

Finally, it should be noted that a systematic difference in the flux observed with open-path and closed-path analyzers for CO₂ at the same site (Ono et al. 2007, 2008b) was not obvious in this study for CH₄. McDermitt et al. (2011) showed that the heat generated by the mirror heaters of an LI-7700 analyzer did not affect the temperature environment in the observational path even under extreme heating conditions. Furthermore, the mirror heaters were switched off in our study. The LI-7700 analyzer may not suffer the heat interference problem that has been observed with the open-path CO₂ analyzer (Burba et al. 2008).

5 Conclusions

Consistency between fluxes observed with the open-path and closed-path eddy-covariance techniques is critical for inter-site comparisons between different ecosystems and allows the cross-validation of fluxes observed with both techniques. The present study clearly demonstrated that the CH₄ fluxes observed using both techniques were consistent. This suggests that the correction procedure proposed to account for the influence of fluctuations in air density and the spectroscopic effect is reasonably accurate, and the approaches used to correct the high-frequency loss that are widely used for the CO₂ flux can be applied to the CH₄ flux also, even when an undersized pump is used with the closed-path CH₄ analyzer. Both the bandpass and transfer function approaches worked well with a careful determination of parameters related to the bandpass frequency region, transfer function, and cospectral shape. This study also re-emphasizes that accurate data processing, specifically the high-frequency loss of the open-path data, is required before these corrections are applied, especially for observations close to the ground. Accuracy in the overall corrections becomes even more important when observing a small CH₄ flux.

Acknowledgments We would like to thank Dr. T. Takimoto for his support in the site maintenance. This work was financially supported in part by JSPS KAKENHI Grant Number 23248023, by the Ministry of Agriculture, Forestry and Fisheries, Japan through a research project (“Development of technologies for mitigation and adaptation to climate change in Agriculture, Forestry and Fisheries”, FY 2010–2014), and also by the Ministry of Environment, Japan through the Global Environment Research Account for National Institutes (“Sensor Network and Data Processing Automation for Evaluation of the Carbon Cycle Change in Terrestrial Ecosystems”, FY 2012–2016). We appreciate comments from the editor and one anonymous reviewer.

Appendix 1: Maximal Overlap Discrete Wavelet Transform

In this study, the coherence among scalars was used in the bandpass approach as described in Sect. 3.2.1. The coherence with the maximal overlap discrete wavelet transform (MODWT) is defined below.

The j th level MODWT coefficients are defined for an arbitrary variable x with a sample size N as follows (Percival and Walden 2000),

$$\tilde{W}_{x,j,t} \equiv \sum_{l=0}^{L_j-1} \tilde{h}_{j,l} x_{t-l \bmod N} \tag{8}$$

for $t = 0, \dots, N - 1$, where $\tilde{h}_{j,l}$ are termed the j th level MODWT wavelet filters and are defined as $h_{j,l}/2^{j/2}$, where $h_{j,l}$ is the j th level wavelet filter; L_j is the width of filters and is defined as $(2^j - 1)(L - 1) + 1$, where L is the width of the $j = 1$ base filter. The cospectrum of w and an arbitrary scalar, x , is given as follows,

$$C_{wx}(f) = \frac{1}{N} \sum_{t=0}^{N-1} \tilde{W}_{w,j,t} \tilde{W}_{x,j,t} \tag{9}$$

where f is defined as $f \equiv 1/(2^j \Delta t)$ with Δt being the sampling interval. The MODWT is a non-orthogonal variant of the discrete wavelet transform (DWT); its decomposition is highly redundant in time. The redundancy of the MODWT coefficients modestly decreases the variance of certain wavelet-based statistical estimates (Cornish et al. 2006). This property may stabilize the characterization of turbulent transfer, especially over the frequency region below the spectral peak frequency.

The coherence between two arbitrary variables (x and y), $\lambda_{xy}(f)$, was calculated using MODWT in a similar way to the DWT version (Scanlon and Albertson 2001) as follows,

$$\lambda_{xy}(f) = \frac{C_{xy}(f)}{\sigma_{x,j} \sigma_{y,j}}, \tag{10}$$

where $\sigma_{x,j}$ is the standard deviation of the j th level MODWT coefficients of variable x .

Wavelet analysis requires the determination of a wavelet filter function, and appropriate selection of the function depends on the objectives of the analysis and the time series being analyzed. We chose the least asymmetric wavelet with eight coefficients, LA(8) (Daubechies 1992), following Cornish et al. (2006). The LA(8) filter has better uncorrelatedness between wavelet coefficients across scales compared to the Haar filter, which has been more commonly used because of its simplicity, and thus the energy leakage problem from nearby frequencies (Qiu et al. 1995) has less influence on the calculated wavelet coefficients.

References

Asakawa T, Kanno N, Tonokura K (2010) Diode laser detection of greenhouse gases in the near-Infrared region by wavelength modulation spectroscopy: pressure dependence of the detection sensitivity. *Sensors* 10:4686–4699

Asanuma J, Ishikawa H, Tamagawa I, Ma Y, Hayashi T, Qi Y, Wang J (2005) Application of the band-pass covariance technique to portable flux measurements over the Tibetan Plateau. *Water Resour Res* 41:W09407

Asanuma J, Tamagawa I, Ishikawa H, Ma Y, Hayashi T, Qi Y, Wang J (2007) Spectral similarity between scalars at very low frequencies in the unstable atmospheric surface layer over the Tibetan plateau. *Boundary-Layer Meteorol* 122:85–103

- Aubinet M, Chermaine B, Vandenhaute M, Longdoz B, Yernaux M, Laitat E (2001) Long term carbon dioxide exchange above a mixed forest in the Belgian Ardennes. *Agric For Meteorol* 108:293–315
- Baer DS, Paul JB, Gupta M, O’Keefe A (2002) Sensitive absorption measurements in the nearinfrared region using off-axis integrated-cavity-output spectroscopy. *Appl Phys B* 75:261–265
- Burba GG, McDermitt DK, Grelle A, Anderson DJ, Xu LK (2008) Addressing the influence of instrument surface heat exchange on the measurements of CO₂ flux from open-path gas analyzers. *Glob Change Biol* 14:1854–1876
- Cornish CR, Bretherton CS, Percival DB (2006) Maximal overlap wavelet statistical analysis with application to atmospheric turbulence. *Boundary-Layer Meteorol* 119:339–374
- Daubechies I (1992) Ten lecture on wavelets. SIAM, Philadelphia, 377 pp
- Dengel S, Levy PE, Grace J, Jones SK, Skiba UM (2011) Methane emissions from sheep pasture, measured with an open-path eddy covariance system. *Glob Change Biol* 17:3524–3533
- Detto M, Verfaillie J, Anderson F, Xu L, Baldocchi D (2011) Comparing laser-based open- and closed-path gas analyzers to measure methane fluxes using the eddy covariance method. *Agric For Meteorol* 151:1312–1324
- Forster P, Ramaswamy V, Artaxo P, Bernsten T, Betts R, Fahey D, Haywood J, Lean J, Lowe D, Myhre G, Nganga J, Prinn R, Raga G, Schulz M, Van Dorland R (2007) Changes in atmospheric constituents and in radiative forcing. *Climate Change 2007: the physical science basis*. Cambridge University Press, Cambridge, U.K., pp 129–234
- Gharavi M, Buckley SG (2005) Diode laser absorption spectroscopy measurement of linestrengths and pressure broadening coefficients of the methane 2ν₃ band at elevated temperatures. *J Mol Spectrosc* 229:78–88
- Grelle A, Lindroth A (1996) Eddy-correlation system for long-term monitoring of fluxes of heat, water vapour and CO₂. *Glob Change Biol* 2:297–307
- Gurvich AS (1962) The pulsation spectra of the vertical component of wind velocity and their relations to the micrometeorological conditions. *Izv Atmos Oceanic Phys* 4:101–136
- Hendriks DMD, Dolman AJ, van der Molen MK, van Huissteden J (2008) A compact and stable eddy covariance set-up for methane measurements using off-axis integrated cavity output spectroscopy. *Atmos Chem Phys* 8:431–443
- Högström U, Bergström H, Smedman A-S, Halldin S, Lindroth A (1989) Turbulent exchange above a pine forest. Part I: fluxes and gradients. *Boundary-Layer Meteorol* 49:197–217
- Horst TW (1973) Spectral transfer functions for a three-component sonic anemometer. *J Appl Meteorol* 12:1072–1075
- Hovde DC, Stanton AC, Meyers TE, Matt DR (1995) Methane emissions from a landfill measured by eddy correlation using a fast response diode laser sensor. *J Atmos Chem* 20:141–162
- Ibrom A, Dellwik E, Flyvbjerg H, Jensen NO, Pilegaard K (2007a) Strong low-pass filtering effects on water vapour flux measurements with closed-path eddy correlation systems. *Agric For Meteorol* 147:140–156
- Ibrom A, Dellwik E, Larsen SE, Pilegaard K (2007b) On the use of the Webb–Pearman–Leuning theory for closed-path eddy correlation measurements. *Tellus* 59B:937–946
- Irwin HPAH (1979) Cross-spectra of turbulence velocities in isotropic turbulence. *Boundary-Layer Meteorol* 16:237–243
- Kaimal JC, Finnigan JJ (1994) Atmospheric boundary layer flows. Oxford University Press, New York 289 pp
- Kaimal JC, Wynagrd JC, Haugen DA (1968) Deriving power spectra from a three-component sonic anemometer. *J Appl Meteorol* 7:827–873
- Kaimal JC, Wyngaard JC, Izumi Y, Coté OR (1972) Spectral characteristics of surface-layer turbulence. *Q J R Meteorol Soc* 98:563–589
- Kosugi Y, Takanashi S, Tanaka H, Ohkubo S, Tani M, Yano M, Katayama T (2007) Evapotranspiration over a Japanese cypress forest. I. Eddy covariance fluxes and surface conductance characteristics for 3 years. *J Hydrol* 337:269–283
- Kristensen L, Jensen NO (1979) Lateral coherence in isotropic turbulence and in the natural wind. *Boundary-Layer Meteorol* 17:353–373
- Laubach J, McNaughton KG (1998) A spectrum-independent procedure for correcting eddy fluxes measured with separated sensors. *Boundary-Layer Meteorol* 89:445–467
- Lee X, Massman W, Law B (eds) (2004) Handbook of micrometeorology. Kluwer, Dordrecht, 250 pp
- Leuning R, Judd MJ (1996) The relative merits of open- and closed-path analyzers for measurement of eddy fluxes. *Glob Change Biol* 2:241–253
- Li-Cor Inc. (2010) Li-7700 open path CH₄ analyzer instruction manual. LI-COR Inc., Lincoln
- Mahrt L (1998) Flux sampling errors for aircraft and towers. *J Atmos Oceanic Technol* 15:416–429
- Mano M, Miyata A, Nagai H, Yamada T, Ono K, Saito M, Kobayashi Y (2007) Random sampling errors in CO₂ fluxes measured by the open-path eddy covariance method and their influence on estimating annual carbon budget’ (in Japanese with English abstract). *J Agric Meteorol* 63:67–79

- Massman WJ (2000) A simple method for estimating frequency response corrections for eddy covariance systems. *Agric For Meteorol* 104:185–198
- Massman WJ, Tuovinen J-P (2006) An analysis and implications of alternative methods of deriving the density (WPL) terms for eddy covariance flux measurements. *Boundary-Layer Meteorol* 121:221–227
- McDermitt D, Burba G, Xu L, Anderson T, Komissarov A, Riensche B, Schedlbauer J, Starr G, Zona D, Oechel W, Oberbauer S, Hastings S (2011) A new low-power, open-path instrument for measuring methane flux by eddy covariance. *Appl Phys B* 102:391–405
- Miyata A, Iwata T, Nagai H, Yamada T, Yoshikoshi H, Mano M, Ono K, Han GH, Harazono Y, Ohtaki E, Baten MA, Inohara S, Takimoto T, Saito M (2005) Seasonal variation of carbon dioxide and methane fluxes at single cropping paddy fields in central and western Japan. *Phyton* 45:89–97
- Moncrieff JB, Massheder JM, de Bruin H, Elbers J, Friborg T, Heusinkveld B, Kabat P, Scott S, Soegaard H, Verhoef A (1997) A system to measure surface fluxes of momentum, sensible heat, water vapour and carbon dioxide. *J Hydrol* 188–189:589–611
- Moore CJ (1986) Frequency response correction for eddy correlation systems. *Boundary-Layer Meteorol* 37:17–35
- Ono K, Hirata R, Mano M, Miyata A, Saigusa N, Inoue Y (2007) ‘Systematic differences in CO₂ fluxes measured by open- and closed-path eddy covariance systems: influence of air density fluctuations resulting from temperature and water vapor transfer’ (in Japanese with English abstract). *J Agric Meteorol* 63:139–155
- Ono K, Mano M, Miyata A, Inoue Y (2008a) Applicability of the planar fit technique in estimating surface fluxes over flat terrain using eddy covariance. *J Agric Meteorol* 64:121–130
- Ono K, Miyata A, Yamada T (2008b) Apparent downward CO₂ flux observed with open-path eddy covariance over a non-vegetated surface. *Theor Appl Climatol* 92:195–208
- Peltola O, Mammarella I, Haapanala S, Burba G, Vesala T (2013) Field intercomparison of four methane gas analyzers suitable for eddy covariance flux measurements. *Biogeosciences* 10:3749–3765
- Percival DB, Walden AT (2000) Wavelet methods for time series analysis. Cambridge University Press, Cambridge, U.K. 594 pp
- Qiu J, Paw UKT, Shaw RH (1995) Pseudo-wavelet analysis of turbulence patterns in three vegetation layers. *Boundary-Layer Meteorol* 72:177–204
- Querino CAS, Smeets CJPP, Viganò I, Holzinger R, Moura V, Gatti LV, Martinewski A, Manzi AO, de Araújo AC, Röckmann T (2011) Methane flux, vertical gradient and mixing ratio measurements in a tropical forest. *Atmos Chem Phys* 11:7943–7953
- Rannik U, Vesala T, Keskinen R (1997) On the damping of temperature fluctuations in a circular tube relevant to the eddy covariance measurement technique. *J Geophys Res* 102:12789–12794
- Rinne J, Riutta T, Pihlatie M, Aurela M, Haapanala S, Tuovinen J-P, Tuittila E-S, Vesala T (2007) Annual cycle of methane emission from a boreal fen measured by the eddy covariance technique. *Tellus* 59B:449–457
- Sachs T, Wille C, Boike J, Kutzbach L (2008) Environmental controls on ecosystem-scale CH₄ emission from polygonal tundra in the Lena River Delta, Siberia. *J Geophys Res* 113:G00A03
- Sachs T, Giebel M, Boike J, Kutzbach L (2010) Environmental controls on CH₄ emission from polygonal tundra on the microsite scale in the Lena river delta, Siberia. *Glob Change Biol* 16:3096–3110
- Saito M, Miyata A, Nagai H, Yamada T (2005) Seasonal variation of carbon dioxide exchange in rice paddy field in Japan. *Agric For Meteorol* 135:93–109
- Saito M, Asanuma J, Miyata A (2007) Dual-scale transport of sensible heat and water vapor over a short canopy under unstable conditions. *Water Resour Res* 43:W05413
- Scanlon TM, Albertson JD (2001) Turbulent transport of carbon dioxide and water vapor within a vegetation canopy during unstable conditions: identification of episodes using wavelet analysis. *J Geophys Res* 106(D7):7251–7262
- Schlesinger WH, Bernhardt ES (2013) Biogeochemistry: an analysis of global change, 3rd edn. Academic Press, San Diego, 671 pp
- Schotanus P, Nieuwstadt FTM, de Bruin HAR (1983) Temperature measurement with a sonic anemometer and its application to heat and moisture fluxes. *Boundary-Layer Meteorol* 26:81–93
- Shaw WJ, Spicer CW, Kenny DV (1998) Eddy correlation fluxes of trace gases using a tandem mass spectrometer. *Atmos Environ* 32:2887–2898
- Shemshad J, Aminossadati SM, Kizil MS (2012) A review of developments in near infrared methane detection based on tunable diode laser. *Sensors Actuators B* 171–172:77–92
- Silverman BA (1968) The effect of spatial averaging on spectrum estimation. *J Appl Meteorol* 7:168–172
- Smeets CJPP, Holzinger R, Viganò I, Goldstein AH, Röckmann T (2009) Eddy covariance methane measurements at a Ponderosa pine plantation in California. *Atmos Chem Phys* 9:8365–8375
- Stull RB (1988) An introduction to boundary layer meteorology. Kluwer, Dordrecht, 666 pp

- Suyker AE, Verma SB, Clement RJ, Billesbach DP (1996) Methane flux in a boreal fen: season-long measurement by eddy correlation. *J Geophys Res* 101:28637–28647
- Tuzson B, Hiller RV, Zeyer K, Eugster W, Neftel A, Ammann C, Emmenegger L (2010) Field intercomparison of two optical analyzers for CH₄ eddy covariance flux measurements. *Atmos Meas Technol* 3:1519–1531
- Verma SB, Ullman FG, Billesbach D, Clement RJ, Kim J, Verry ES (1992) Eddy correlation measurements of methane flux in a northern peatland ecosystem. *Boundary-Layer Meteorol* 58:289–304
- Vickers D, Mahrt L (1997) Quality control and flux sampling problems for tower and aircraft data. *J Atmos Oceanic Technol* 14:512–526
- Watanabe T, Yamanoi K, Yasuda Y (2000) Testing of the bandpass eddy covariance method for a long-term measurement of water vapour flux over a forest. *Boundary-Layer Meteorol* 96:473–491
- Webb EK, Pearman GI, Leuning R (1980) Correction of flux measurements for density effects due to heat and water vapour transfer. *Q J R Meteorol Soc* 106:85–100
- Yasuda Y, Watanabe T (2001) Comparative measurements of CO₂ flux over a forest using closed-path and open-path CO₂ analyzers. *Boundary-Layer Meteorol* 100:191–208
- Zona D, Oechel WC, Kochendorfer J, Paw UKT, Salyuk AN, Olivas PC, Oberbauer SF, Lipson DA (2009) Methane fluxes during the initiation of a large-scale water table manipulation experiment in the Alaskan Arctic tundra. *Glob Biogeochem Cycles* 23:GB2013